Magazine of Concrete Research
Volume 66 Issue 24

Curvature-relevant analysis of eccentrically loaded circular concrete-filled steel tube columns
Ouyang and Ho

Magazine of Concrete Research, 2014, **66**(24), 1263–1276
http://dx.doi.org/10.1680/macr.14.00112
Paper 1400112
Received 10/04/2014; revised 24/07/2014; accepted 30/07/2014
Published online ahead of print 11/09/2014

ice
Institution of Civil Engineers
publishing

Curvature-relevant analysis of eccentrically loaded circular concrete-filled steel tube columns

Yi Ouyang
PhD Candidate, Department of Civil Engineering, The University of Hong Kong, Hong Kong, PR China

Johnny Ching Ming Ho
Senior Lecturer, School of Civil Engineering, The University of Queensland, Brisbane, Australia

The existence of curvature can reduce the effective confining pressure within concrete-filled steel tube (CFST) columns under eccentric compression. The existing analysis method ignores such an effect and still treats the confining pressure as constant across the whole section as if it is under axial compression. In this paper, the authors have made significant improvements on the existing model, so that the curvature effect can be taken into account to properly interpret the non-linear behaviour of eccentrically loaded CFST columns. Meanwhile, shortening between two hinges is an important data output in test programmes of this type, which has been completely neglected by the existing analysis method. This improved method also provides calculation steps to track the value of shortening for each load increment. Unknown parameters in this new method are determined on the basis of data fitting of 87 specimens from previous researchers' test programmes. The following parameters are incorporated in this study: effective tube length (660–4670 mm), diameter of tube (76–600 mm), tube thickness (1·52–8·81 mm), yield strength of tube (256·4–517·0 MPa), cylinder strength of concrete (26·42–112·70 MPa) and eccentricity (9·4–300 mm). The load–axial displacement, load–deflection and moment–curvature curves predicted by the new method agree well with their measured counterparts in the tests.

Notation

$A_{c,i}$	area of concrete element i
$A_{s,j}$	area of steel element j
D	outer diameter of steel tube
d_e	axial deformation along the loading axis
d_i	depth of concrete element i
d_j	depth of steel element j
d_n	neutral axis depth
E_s	elastic modulus of steel
e	eccentricity
f_c	cylinder concrete strength
f_{cc}	confined concrete strength
f_r	confining pressure
$f_{r,avg}$	average mean confining pressure across concrete core
$f_{r,eff}$	effective confining pressure
f_y	yield stress of steel
f_{yc}	compressive yield stress of steel in biaxial stress state
f_{yt}	tensile yield stress of steel in biaxial stress state
L	original hinge–hinge length of CFST column
L_s	original specimen length of CFST column
L_s'	reduced specimen length of CFST column
M	internal moment
P	eccentric load
t	thickness of steel tube
u	deflection of eccentrically loaded circular CFST column
u_i	deflection component due to inclination of experimental set-up
u_m	mid-span deflection of eccentrically loaded circular CFST column
u_s	deflection component due to deformation of specimen
$u_{s,m}$	amplitude of assumed sine wave deflection shape
Δ	deflection
ε	strain
ε_c	strain corresponding to peak unconfined concrete stress
ε_{cc}	strain corresponding to peak confined concrete stress
$\varepsilon_{c,i}$	strain of concrete element i
ε_e	strain at mid-span of eccentricity axis
$\varepsilon_{s,j}$	strain of steel element j
θ	inclination angle of experimental set-up
ρ	steel content in eccentrically loaded circular CFST column
σ	stress
σ_c	stress in concrete
$\sigma_{c,i}$	stress in concrete element i
σ_h'	effective hoop stress in steel tube
σ_s	longitudinal stress in steel tube
$\sigma_{s,j}$	longitudinal stress in steel element j
Φ	reduction factor of effective confining pressure due to curvature
ϕ	curvature of eccentrically loaded circular CFST column
ϕ_m	mid-span curvature of eccentrically loaded circular CFST column

Introduction

High-performance concrete (HPC), including ultra high-strength concrete (UHSC), has recently attracted a lot of attention in academic research and practical construction design thanks to its superior performance such as improved strength and stiffness, workability, durability, water-, impact- and blast-resistance, cohesiveness, self-levelling and self-compacting abilities, etc. With the advancement of powder and filler technologies (Iveson *et al.*, 2001), the evolution of ultrafine materials (Kwan and Ng, 2010) and new wet packing and excess water theories (Wong and Kwan, 2008a, 2008b), HPC can be easily produced without a significant cost increase when compared with ordinary normal-strength concrete. Furthermore, by adopting appropriate apportionment between cementitious and non-cementitious ingredients, as well as a suitable dosage of superplasticiser to achieve maximum packing density under wet conditions (Kwan and Fung, 2009), HPC can be designed to have less carbon footprint than normal concrete (Kayali, 2008). Nevertheless, despite all these advantages, HPC loses ductility as its strength increases. This is one of the major reasons why the practical application of HPC is so limited.

To practically use UHSC without jeopardising the ductility performance of structures, appropriate confinement should be provided to the UHSC. Traditionally in reinforced concrete structures, this is provided by installing closely spaced transverse steel (Ho and Pam, 2003; Mander *et al.*, 1988). However, as the efficiency of transverse reinforcement dropped significantly with the increase in concrete strength (Ho *et al.*, 2010), this form of confinement will result in serious steel congestion that adversely affects the concrete placing quality, and is not applicable to confine UHSC. To effectively confine UHSC and at the same time maintain concrete placing quality, concrete-filled steel tube (CFST) construction has been proposed. This technique is very efficient in confining members subjected to combined axial load and flexure (e.g. columns). In CFST columns, the concrete core is effectively confined by the circumventing steel tube via the transverse strain compatibility between the concrete and steel after the concrete has cracked. Since the free lateral dilation of the concrete core is significantly larger than that of the steel tube after concrete cracks start to emerge, passive confinement with variable pressure exerted by the steel tube on the concrete core is triggered in the loading process, which enhances the strength and ductility of the confined concrete.

Because of the variation of concrete dilation at different loading stages, the confining pressure varies. However, in some previous research studies on CFST columns (Attard and Setunge, 1996; Johansson and Gylltoft, 2001; Richart *et al.*, 1929), it has been reported that the response of concrete under passive confinement is similar to that under active confinement, where the confinement pressure is treated as constant. Therefore, despite the fact that the real-time pressure in a CFST column is difficult to trace, it is reasonable to analyse the flexural behaviour of a CFST by a constant confining pressure throughout the loading process (Hajjar *et al.*, 1998; Hatzigeorgiou, 2008). Subsequently, many different empirical equations have been developed to correlate the pressure with various material properties and geometry of the cross-section of CFST columns (Hatzigeorgiou, 2008; Hu *et al.*, 2003; Tang *et al.*, 1996).

Circular, square and rectangular sections are the most commonly adopted CFST column cross-sections. Because of the radial confining pressure acting in the circular concrete core (Hatzigeorgiou, 2008; Johansson, 2002; Suthansa *et al.*, 2001), circular CFST columns are much better confined than square and rectangular CFST columns (Lee *et al.*, 2011; Oliveira *et al.*, 2010) under uniaxial compression. Nevertheless, arching action will be developed in the plane of cross-section between the corners of the steel tube, where the restraint provided to concrete is the largest, due to tube bending. Furthermore, buckling between these laterally restrained points can easily occur under compression, which weakens the confining pressure and leads to faster strength degradation (Bridge and O'Shea, 1998; Tao *et al.*, 2007; Uy, 2000).

Nonetheless, when a CFST column is subjected to simultaneous axial load and flexure, there is a remarkable loss in the confinement effect due to the increasing curvature of the cross-section, even for circular sections (Johansson and Gylltoft, 2001; Portoles *et al.*, 2011). There have been many experimental studies on the behaviour of circular CFST columns, which can be classified as columns subjected to constant eccentricity with increasing moment and axial load (Kilpatrick and Rangan, 1999; Lee *et al.*, 2011; Muciaccia *et al.*, 2011; O'Shea and Bridge, 2000; Portoles *et al.*, 2011, 2013) and columns subjected to constant axial load and increasing moment with constant axial load (Fujimoto *et al.*, 2004; Inai *et al.*, 2004; Prion and Boehme, 1994). In an eccentrically loaded specimen, axial and flexural deformations will increase as the axial load increases whereas in the second type of test specimen, axial deformation has been exerted upon the column before flexure starts to rise. Accordingly, analysis on the flexural behaviour of these two types of test needs different modelling techniques: those programmes designed for the first type may not be able to accurately interpret the test results of the second type. And because of the increasing flexural deformation, the second-order P–Δ effect will increase and hence so will the moment subjected by the columns. These factors should be included in analytical models for predicting the flexural capacity of CFST columns.

Due to the second-order P–Δ effect, the moment capacity in CFST columns increases with flexural deflection. After the concrete has reached the ultimate concrete strain and starts to crack, which is later confined by the steel tube, flexural deformation increases significantly, hence the loss in secondary moment. In order to predict the moment capacity of flexural CFST columns more accurately, the flexural deflection should be assessed. Previously, work has been done by other researchers to evaluate the deflected shape of CFST columns based on the part-cosine wave model (Neogi *et al.*, 1969) and the half-sine wave model (Liang, 2011). However, no axial deformation is taken into

account in these models and hence they overestimate the deflected shape as well as the moment capacity of CFST columns. In this paper, a new non-linear analysis method, which can track the axial deformation during the eccentric loading process, is proposed to evaluate the overall behaviour of eccentrically loaded circular CFST columns (e.g. eccentric load against axial displacement curves, eccentric load against mid-span deflection curve and mid-span moment against curvature).

In Liang's previous model on eccentrically loaded CFST columns (Liang, 2011), the confining pressure is treated as constant across the whole section and throughout the entire loading process. Although this model can deliver analytical results sufficiently close to the test results, it does not properly reflect the mechanism of eccentrically loaded CFST columns. In this paper, a new constitutive model for confined concrete in eccentrically loaded circular CFST columns is developed to account for the loss of effective confinement due to flexural deformation. The parameters in the proposed model are determined by data fitting of a total number of 87 specimens extracted from previous researchers' test programmes. It is evident that the eccentric loading capacities predicted by the proposed model agree well with the measured results in the tests. By comparing the obtained theoretical results with those evaluated by the non-linear analysis model of Liang (2011), it is shown that the proposed model can predict more accurately the flexural behaviour of CFST columns subjected to eccentric axial load.

Proposed stress–strain relation for CFST concrete under eccentric loading

The stress–strain model proposed by Attard and Setunge (1996) is adopted in this paper to model the behaviour of concrete under eccentric load. The model is

$$Y = \frac{AX + BX^2}{1 + CX + DX^2} \qquad Y = \frac{\sigma}{f_{cc}} \qquad X = \frac{\varepsilon}{\varepsilon_{cc}} \tag{1}$$

Two sets of values for coefficients A, B, C and D are determined in Equation 1 to represent the ascending branch and descending branch respectively (Attard and Setunge, 1996). These procedures are not covered in detail in this paper.

From Equation 1, it is evident that the ascending portion of the stress–strain curve is defined by the point of maximum concrete stress f_{cc} and the corresponding concrete strain ε_{cc}. These can be determined using the equations of Richart *et al.* (1928)

$$f_{cc} = f_c + k_1 f_r \tag{2}$$

$$\varepsilon_{cc} = \varepsilon_c \left(1 + k_2 \frac{f_r}{f_c}\right) \tag{3}$$

where f_c is the unconfined cylinder strength for concrete and its corresponding strain ε_c. The values of k_1 and k_2 vary in different publications. In this paper, the recommendations of Mander *et al.* (1988) are adopted ($k_1 = 4{\cdot}1$ and $k_2 = 20{\cdot}5$).

As suggested by Equation 2, f_{cc} is the maximum concrete stress attained under the effect of confining pressure f_r. For circular CFST columns under uniaxial compression, the confining pressure can be easily evaluated by considering force equilibrium within the cross-section and is considered to have the same value on both minor axes from the perspective of triaxial stress state. However, the confining pressure will reduce in bending because curvature exists and the concrete is no longer subjected to uniform compressive stress (Johansson and Gylltoft, 2001). Besides, the confining pressure f_r along the two minor axes will be different (i.e. $f_{r,2}$ and $f_{r,3}$). Based on these facts, the following assumptions are made to facilitate the modelling of concrete under eccentric loading.

(*a*) Although the confining pressure in a circular CFST column under eccentric loading varies during the loading process in different directions and positions of the concrete core, a representative average mean value of the confining pressure obtained from Equation 4

$$f_{r,avg} \approx \int_{A_c} [(f_{r,2} + f_{r,3})/2] \, dA_c / A_c \tag{4}$$

can be assumed so that an effective hoop stress (σ'_h) in steel can be calculated.

(*b*) From the test results obtained by Kupfer *et al.* (1969), the biaxial strength of concrete is $1{\cdot}16f_c$, which means that when $f_{r,2} = 1{\cdot}16f_c$ and $f_{r,3} = 0$, $f_{cc} = 1{\cdot}16f_c$. Meanwhile, Equation 2 gives $f_{cc} = 3{\cdot}38f_c$ when $f_{r,2} = f_{r,3} = 0{\cdot}58f_c$. This phenomenon has been well explained by Menétrey and Willam's triaxial failure criterion (Menétrey and Willam, 1995) and the extended Drucker–Prager failure criterion (Yu *et al.*, 2010) for concrete. Even if the mean value of $f_{r,2}$ and $f_{r,3}$ remains the same, the larger difference between their actual values will end up with a weaker effective confinement. Therefore, the effective confining pressure can be related to a curvature-dependent reduction factor Φ (i.e. $f_{r,eff} = \Phi f_{r,avg}$; $0 < \Phi \leqslant 1$), and used in Equation 2 to determine f_{cc}.

(*c*) Confining pressure within the extreme compressive concrete fibre will be $f_{r,eff}$, and will be linearly decreasing until it reaches zero at the neutral axis depth d_n.

The confining pressure within the CFST should obviously be affected by the area ratio of steel/total area of the CFST cross-

section. When there is no steel tube, meaning it is bare concrete, the confining pressure is zero. By adding an amount of steel, the confining pressure will increase but with a returning slope so that, to some extent, the benefit from adding steel area is limited. On the other hand, a steel tube with a higher yield strength should produce a larger confining pressure within the CFST. Therefore, it is proposed that the empirical value of $f_{r,avg}$ can be directly obtained using Equations 4 and 5, which increases with steel content ρ and the yield strength of steel f_y. Equation 4 fulfils the boundary condition that there should not be any confining pressure when $\rho = 0$.

$$4. \quad f_{r,avg} = a_1 \ln(a_2\rho + 1) f_y \leqslant \frac{2tf_y}{D - 2t}$$

$$5. \quad \rho = 1 - \left(1 - \frac{2t}{D}\right)^2$$

Between two specimens with the same tube diameter and thickness but different slenderness ratios or eccentricities, the one with the larger slenderness ratio or eccentricity will attain less effective confinement from the tube since it experiences larger curvature during the loading process. When the curvature of the CFST section continues to build up, the concrete will keep losing effective confinement and the effective confining pressure will approach zero slowly. Such a mechanism can be explained by the reduction factor Φ in assumption (b), and it is reasonable to assume Φ decreases with curvature ϕ. When the curvature increases due to the second-order P–Δ effect, the growing curvature will magnify the difference between $f_{r,2}$ and $f_{r,3}$, and hence reduce $f_{r,eff}$. Therefore, Equation 6 is proposed. It should be noted that when $\phi = 0$, which indicates axial compression state, $\Phi = 1$ and when $\phi \to \infty$, $\Phi \to 0$.

$$6. \quad \Phi = \exp(-b_1\phi)$$

During the analysis process, the curvature of the eccentrically loaded CFST column was increased sequentially, so that the value of Φ needs to be re-evaluated after each loading step. As a result, even if the parameters concerning the loading configurations (e.g. slenderness ratio and eccentricity) are not explicitly included in Equation 6, they will change the increasing path of ϕ and the position of the neutral axis, thereby changing the decreasing path of Φ, as well as the confining pressure profile of the concrete core as per assumption (c). Details of the analysis process will be discussed later in the paper. The parameters a_1, a_2 and b_1 in Equations 4 and 6 will be determined using 87 CFST specimens from the literature and these will also be further discussed in detail later in this paper.

Stress–strain relation for steel

A linearly-elastic perfectly-plastic model is adopted to represent the stress–strain relationship of the steel tube. To be conservative, strength hardening in steel is neglected in this paper. Nevertheless, since the steel tube in a CFST column is subjected to a biaxial stress state, the longitudinal yield strength is not equal to the uniaxial yield strength. Under compression, the concrete dilates and induces tensile hoop stress in the steel tube, which in turn confines the concrete core. Consequently, the yield strength that can be developed by the steel tube is less than the uniaxial yield strength. Since steel is a ductile material, the von Mises failure criteria can be adopted to evaluate the longitudinal yield strength of steel tube under the effective hoop tensile stress, as shown in Figure 1 (compression taken as positive). The formulas for evaluating the tensile and compressive yield strength of the steel tube under a biaxial stress state are

$$7. \quad f_{yt} = 0{\cdot}5[\sigma'_h - (4f_y^2 - 3\sigma'^2_h)^{1/2}]$$

$$8. \quad f_{yc} = 0{\cdot}5[\sigma'_h + (4f_y^2 - 3\sigma'^2_h)^{1/2}]$$

$$9. \quad \sigma'_h = f_{r,avg}\frac{(D - 2t)}{2t}$$

where compression is taken as positive. The Young's modulus of the steel tube is taken always equal to 200 GPa.

Non-linear analysis method

Fibre element analysis

To compute the resultant force and moment within the cross-section of a CFST column, the most accurate way is to apply continuous integration over the whole cross-section; the computation cost of this will be extremely high. Therefore, in this paper the cross-section is divided into finite fibre elements for analysis purposes. The fibre element method, with the assumption that plane sections remain plane during the loading process, can deliver results efficiently with satisfactory accuracy for circular CFST columns (Liang, 2011).

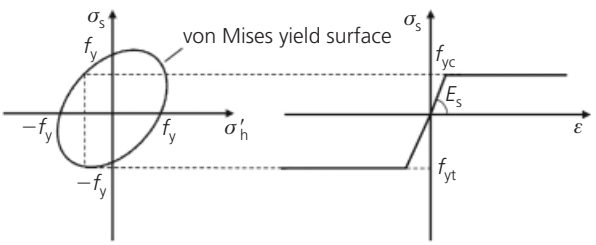

Figure 1. Stress–strain relation for steel tubes

The concrete core is divided into laminar elements while the steel tube is divided into radial elements (see Figure 2). Laminar elements in the concrete core can reduce the number of total elements, compared with radial elements, since the strain is the same across one layer; radial elements in the circular steel tubes have a simpler rule for discretisation than laminar ones. The strain of concrete element i (or steel element j) at depth d_i (or d_j) can be calculated once the depth of the neutral axis d_n and the curvature of the cross-section ϕ are known

$$\varepsilon_{c,i} = \phi(d_n - d_i)$$

10. $$\varepsilon_{s,j} = \phi(d_n - d_j)$$

where the sign convention is positive for compression and negative for tension.

After obtaining the strain for each element, the corresponding stress can be mapped by applying the constitutive stress–strain relations for each material. The resultant force and internal moment of the cross-section can be then be calculated from

11. $$P = \sum_{i=1}^{n} \sigma_{c,i} A_{c,i} + \sum_{j=1}^{m} \sigma_{s,j} A_{s,j}$$

12. $$M = \sum_{i=1}^{m} \sigma_{c,i} A_{c,i} \left(\frac{D}{2} - d_i\right) + \sum_{j=1}^{m} \sigma_{s,j} A_{s,j} \left(\frac{D}{2} - d_j\right)$$

where n and m are respective total numbers of concrete elements and steel elements.

Deflection shape of eccentrically loaded CFST columns

When a CFST column specimen is loaded eccentrically, the horizontal deflection for the entire specimen increases as its axial deformation builds up. Normally, the most critical deflection happens at the mid-span of the specimen, and the internal moment within the cross-section of the specimen continues to build up even if sometimes the eccentric load has already dropped (Portoles *et al.*, 2011). Therefore, the secondary moment due to the P–Δ effect is an important consideration for the nonlinear analysis of CFST columns under eccentric loading. Previous research assumed a half-circle sine wave curve between the two hinges to model the deflection shape of both short (Lee *et al.*, 2011) and slender (Liang, 2011) columns under eccentric loading. However, it is more reasonable to consider part of the specimen length in the half-circle sine wave curve and the rest of the effective concrete length L (the top and bottom steel plates and other test set-ups) a rigid link, as illustrated in Figure 3. As a result, the horizontal deflection at any location of the specimen is divided into two parts – one is due to the deformation of the specimen and the other the inclination of the set-ups. This can be expressed by the following equations.

13. $$u = u_s + u_i = u_{s,m} \sin\left(\frac{\pi z}{L_s'}\right) + \frac{L - L_s}{2} \sin\theta$$

14. $$u_s = u_{s,m} \sin\left(\frac{\pi z}{L_s'}\right)$$

15. $$u_i = \frac{L - L_s}{2} \sin\theta$$

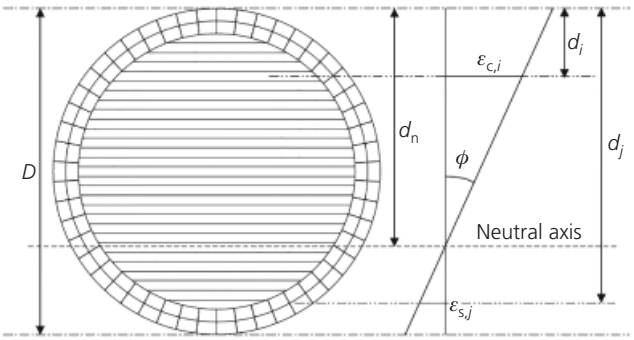

Figure 2. Fibre element discretisation of mid-span section

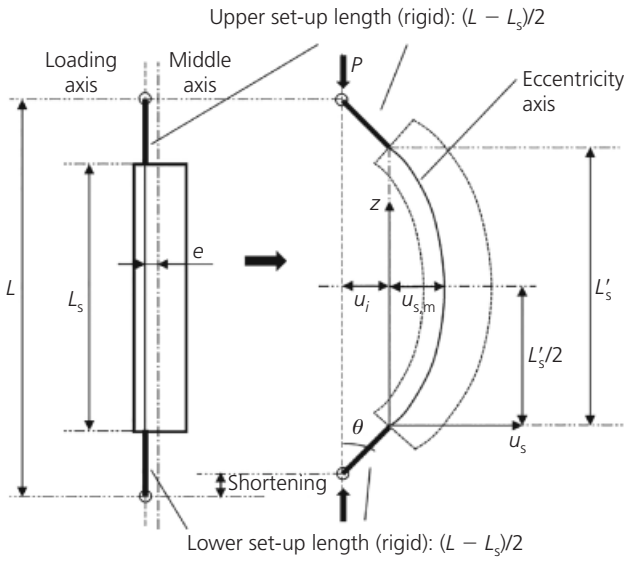

Figure 3. Assumed deformation shape for eccentrically loaded circular CFST columns

$$16.\quad \sin\theta = \frac{u_{s,m}\pi}{L_s'[1+(u_{s,m}\pi/L_s')^2]^{1/2}}$$

where the use of L_s' instead of L_s is because the actual column length is shortened due to longitudinal shortening and bending of the specimen.

In order to analyse the most critical position of the CFST columns, the deflection and curvature at the mid-point of the specimen are calculated as

$$17.\quad u_m = u_{s,m} + \frac{L-L_s}{2}\sin\theta$$

$$18.\quad \phi_m = \left|\frac{d^2u_s}{dz^2}|_{z=L_s'/2}\right| = \left(\frac{\pi}{L_s'}\right)^2 u_{s,m}$$

The neutral axis depth d_n of the cross-section at the mid-point of the specimen is determined by numerical iteration, such as the

Reference	Specimen ID	L: mm	L_s: mm	D: mm	t: mm	f_y: MPa	f_c: MPa	e: mm	P_e: kN	P_{Liang}/P_e	P_{model}/P_e
Neogi *et al.* (1969)											
	M1	3327·4	3048·0	169·42	5·11	308·9	45·6	47·6	621·8	1·00	0·93
	M2	3327·4	3048·0	169·16	5·26	308·9	43·8	38·1	701·5	0·97	0·91
	M3	3327·4	3048·0	168·91	5·66	295·0	33·4	47·6	599·8	0·99	0·92
	M4	3327·4	3048·0	168·40	6·55	298·1	30·6	47·6	624·7	1·01	0·95
	M5	3327·4	3048·0	169·16	7·19	312·0	26·4	47·6	652·6	1·04	0·98
	M6	3327·4	3048·0	169·16	7·29	312·0	27·3	38·1	738·3	1·02	0·97
	M7	3302·0	3022·6	168·91	8·81	322·8	27·2	47·6	757·3	1·03	1·00
Kilpatrick and Rangan (1999)											
	SC-0	802·0	622·0	76·00	2·20	435·0	58·0	15·0	246·0	1·10	0·91
	SC-1	1032·0	852·0	76·00	2·20	435·0	58·0	15·0	208·0	1·13	0·97
	SC-2	1262·0	1082·0	76·00	2·20	435·0	58·0	15·0	184·0	1·11	0·98
	SC-3	1487·0	1307·0	76·00	2·20	435·0	58·0	15·0	162·0	1·11	1·00
	SC-4	1717·0	1537·0	76·00	2·20	435·0	58·0	15·0	141·0	1·11	1·02
	SC-5	1947·0	1767·0	76·00	2·20	435·0	58·0	15·0	121·0	1·13	1·06
	SC-6	2172·0	1992·0	76·00	2·20	435·0	58·0	15·0	107·0	1·13	1·07
	SC-7	2402·0	2222·0	76·00	2·20	435·0	58·0	15·0	96·0	1·10	1·05
	SC-9	1947·0	1767·0	101·70	2·40	410·0	58·0	10·0	361·0	1·02	0·92
	SC-10	1947·0	1767·0	101·70	2·40	410·0	58·0	15·0	309·0	1·04	0·93
	SC-11	1947·0	1767·0	101·70	2·40	410·0	58·0	20·0	275·0	1·05	0·93
	SC-12	1947·0	1767·0	101·70	2·40	410·0	58·0	25·0	240·0	1·08	0·97
	SC-13	1947·0	1767·0	101·70	2·40	410·0	58·0	30·0	220·0	1·08	0·97
	SC-14	1947·0	1767·0	101·70	2·40	410·0	58·0	40·0	188·0	1·06	0·97
	SC-15	1947·0	1767·0	101·70	2·40	410·0	58·0	50·0	158·0	1·08	0·99
O'Shea and Bridge (2000)											
	S30E150B	661·5	580·0	165·00	2·82	363·3	48·3	17·2	1123·0	1·04	0·96
	S30E280A	661·0	579·5	165·00	2·82	363·3	80·2	9·4	1904·0	0·93	0·91
	S30E180A	661·0	579·5	165·00	2·82	363·3	80·2	17·9	1653·0	0·95	0·91
	S30E110B	660·0	578·5	165·00	2·82	363·3	112·7	15·6	1880·0	1·09	1·07
	S16E150B	743·5	662·0	190·00	1·52	306·1	48·3	15·5	1260·0	0·96	0·95
	S16E180A	745·0	663·5	190·00	1·52	306·1	80·2	14·3	1925·0	0·95	0·98
	S16E110B	742·0	660·5	190·00	1·52	306·1	112·7	12·9	2420·0	1·03	1·08
	S20E150A	745·5	664·0	190·00	1·94	256·4	41·0	16·2	1284·0	0·85	0·84
	S20E280B	744·0	662·5	190·00	1·94	256·4	74·7	10·0	2203·0	0·84	0·87
	S20E180B	744·5	663·0	190·00	1·94	256·4	74·7	20·8	1730·0	0·92	0·94
	S20E110B	746·0	664·5	190·00	1·94	256·4	112·7	17·0	2386·0	0·99	1·03

Table 1. Data of eccentrically loaded circular-sectioned CFST specimens (continued on next page)

Reference	Specimen ID	L: mm	L_s: mm	D: mm	t: mm	f_y: MPa	f_c: MPa	e: mm	P_e: kN	P_{Liang}/P_e	P_{model}/P_e
Lee *et al.* (2011)											
	O49E24_30	1400·0	720·0	240·00	6·00	489·0	31·5	120·0	1277·0	1·13	1·00
	O49E36_30	1760·0	1080·0	360·00	6·00	498·0	31·5	60·0	4294·0	1·02	0·99
	O49E48_30	2120·0	1440·0	480·00	6·00	468·0	31·5	240·0	3323·0	1·04	0·98
	O49E60_30	2480·0	1800·0	600·00	6·00	517·0	31·5	300·0	4590·0	1·09	1·01
	O49E24_60	1400·0	720·0	240·00	6·00	489·0	59·0	120·0	1438·0	1·18	1·07
	O49E36_60	1760·0	1080·0	360·00	6·00	498·0	59·0	180·0	2537·0	1·14	1·10
	O49E48_60	2120·0	1440·0	480·00	6·00	468·0	59·0	240·0	3895·0	1·09	1·05
Muciaccia *et al.* (2011)											
	NVC-80-1	1310·0	800·0	139·60	4·00	374·0	62·0	25·0	756·9	1·23	1·09
	NVC-80-2	1230·0	800·0	139·60	4·00	374·0	62·0	25·0	874·7	1·09	0·95
	NVC-200-1	2125·0	1855·0	139·60	4·00	374·0	62·0	25·0	608·2	1·18	1·07
	NVC-200-2	2135·0	1865·0	139·60	4·00	374·0	62·0	25·0	605·7	1·18	1·07
	NVC-300-1	3270·0	3000·0	139·60	4·00	374·0	62·0	25·0	555·9	0·90	0·84
	NVC-300-2	3270·0	3000·0	139·60	4·00	374·0	62·0	25·0	484·1	1·03	0·97
	NVC-440-1	4670·0	4400·0	139·60	4·00	374·0	62·0	25·0	336·2	0·97	0·94
	NVC-440-2	4670·0	4400·0	139·60	4·00	374·0	62·0	25·0	333·0	0·98	0·95
Portoles *et al.* (2011)											
	C100-3-2-30-20-1	2135·0	2000·0	100·00	3·00	322·0	32·7	20·0	181·6	1·23	1·12
	C100-3-2-30-50-1	2135·0	2000·0	100·00	3·00	322·0	34·5	50·0	117·5	1·20	1·11
	C100-3-2-70-20-1	2135·0	2000·0	100·00	3·00	322·0	65·8	20·0	248·6	1·07	0·98
	C100-3-2-70-50-1	2135·0	2000·0	100·00	3·00	322·0	71·6	50·0	151·6	1·05	0·99
	C100-3-2-90-20-1	2135·0	2000·0	100·00	3·00	322·0	95·6	20·0	271·0	1·08	1·01
	C100-3-2-90-50-1	2135·0	2000·0	100·00	3·00	322·0	93·0	50·0	154·2	1·07	1·02
	C100-3-3-30-20-1	3135·0	3000·0	100·00	3·00	322·0	39·4	20·0	140·3	1·15	1·08
	C100-3-3-30-50-1	3135·0	3000·0	100·00	3·00	322·0	36·7	50·0	93·8	1·15	1·07
	C100-3-3-70-20-1	3135·0	3000·0	100·00	3·00	322·0	71·7	20·0	159·6	1·10	1·05
	C100-3-3-70-50-1	3135·0	3000·0	100·00	3·00	322·0	79·6	50·0	102·8	1·14	1·10
	C100-3-3-90-20-1	3135·0	3000·0	100·00	3·00	322·0	94·6	20·0	160·3	1·16	1·10
	C100-3-3-90-50-1	3135·0	3000·0	100·00	3·00	322·0	90·4	50·0	106·8	1·11	1·07
	C100-5-2-30-20-1	2135·0	2000·0	100·00	5·00	322·0	35·4	20·0	270·0	1·14	1·07
	C100-5-2-30-50-1	2135·0	2000·0	100·00	5·00	322·0	30·5	50·0	161·3	1·21	1·14
	C100-5-2-70-20-1	2135·0	2000·0	100·00	5·00	322·0	70·2	20·0	313·6	1·10	1·04
	C100-5-2-70-50-1	2135·0	2000·0	100·00	5·00	322·0	61·0	50·0	183·8	1·16	1·11
	C100-5-2-90-20-1	2135·0	2000·0	101·60	5·00	320·0	95·4	20·0	330·4	1·16	1·10
	C100-5-2-90-50-1	2135·0	2000·0	101·60	5·00	320·0	81·7	50·0	213·5	1·08	1·04
	C100-5-3-30-20-1	3135·0	3000·0	101·60	5·00	320·0	38·7	20·0	212·5	1·10	1·05
	C100-5-3-30-50-1	3135·0	3000·0	101·60	5·00	320·0	39·6	50·0	144·8	1·09	1·06
	C100-5-3-70-20-1	3135·0	3000·0	101·60	5·00	320·0	71·9	20·0	231·4	1·08	1·04
	C100-5-3-70-50-1	3135·0	3000·0	101·60	5·00	320·0	72·5	50·0	153·2	1·12	1·07
	C100-5-3-90-20-1	3135·0	3000·0	101·60	5·00	320·0	86·4	20·0	246·8	1·04	1·00
	C100-5-3-90-50-1	3135·0	3000·0	101·60	5·00	320·0	96·7	50·0	165·0	1·07	1·03
	C125-5-3-90-20-1	3135·0	3000·0	125·00	5·00	322·0	88·0	20·0	474·2	0·99	0·94
	C125-5-3-90-50-1	3135·0	3000·0	125·00	5·00	322·0	97·0	50·0	317·9	1·00	0·96
	C125-5-3-90-20-2	3135·0	3000·0	125·00	5·00	322·0	107·3	20·0	489·5	0·99	0·95
	C125-5-3-90-50-2	3135·0	3000·0	125·00	5·00	322·0	97·9	50·0	323·0	0·98	0·94
	C160-6-3-90-20-1	3135·0	3000·0	160·10	5·70	322·0	87·4	20·0	1012·5	0·97	0·93
	C160-6-3-70-50-1	3135·0	3000·0	160·10	5·70	322·0	74·8	50·0	642·2	1·01	0·96
	C160-6-3-90-20-2	3135·0	3000·0	160·10	5·70	322·0	83·1	20·0	1011·5	0·96	0·92
	C160-6-3-90-50-1	3135·0	3000·0	160·10	5·70	322·0	98·5	50·0	686·2	1·00	0·96

Table 1. (continued on next page)

Reference	Specimen ID	L: mm	L_s: mm	D: mm	t: mm	f_y: MPa	f_c: MPa	e: mm	P_e: kN	P_{Liang}/P_e	P_{model}/P_e
Xue *et al.* (2012)											
	N3-0-E	820·0	700·0	219·00	3·00	313·0	51·8	50·0	1457·0	0·94	0·91
	N4-0-E	820·0	700·0	219·00	4·00	313·0	51·8	50·0	1634·0	0·94	0·90
	N5-0-E	820·0	700·0	219·00	5·00	313·0	51·8	50·0	1874·0	0·99	0·86
Portoles *et al.* (2013)											
	C-HSC-50	2135·0	2000·0	159·00	6·00	376·0	75·7	50·0	870·0	1·05	0·98
	C-UHSC-20	2135·0	2000·0	159·00	6·00	380·0	109·8	20·0	1462·0	1·06	0·99
	C-UHSC-20-b	2135·0	2000·0	159·00	6·00	487·0	110·7	20·0	1525·0	1·14	1·05
	C-UHSC-50	2135·0	2000·0	159·00	6·00	444·0	91·4	50·0	1033·0	1·02	0·95
Mean										1·06	1·00
Standard deviation										0·082	0·069
Coefficient of variance: %										8·00	6·54

Table 1. (continued)

secant method (Liang, 2011) or Newton's method, until the following equilibrium of internal moment is fulfilled

$$M = P(u_m + e) \tag{19}$$

Axial shortening of the CFST column specimens

In previous research, shortening of the actual specimen length is not considered (Liang, 2011) and L_s' is taken as equal to L_s. However, the value of L_s' can be determined if the solution of the following equation can be found

$$\int_0^{L_s'} I_A \, dz = L_s(1 - \varepsilon_e) \tag{20}$$

$$\varepsilon_e = \phi_m\left(d_n - \frac{D}{2} + e\right) \tag{21}$$

$$I_A = \left\{1 + \left[\frac{u_{s,m}\pi}{L_s'}\cos\left(\frac{\pi z}{L_s'}\right)\right]^2\right\}^{1/2} \tag{22}$$

where L_s' is the unknown to be solved for. Integration of the left-hand side of Equation 20 gives the arc length of the longitudinal fibre on the eccentricity axis of the specimen, while the right-hand side is also the same arc length based on the assumption that the original length L_s of that fibre is shortened by the amount of compressive strain at the mid-point of that fibre.

Since it will be very hard to find an analytical integration for the left-hand side of Equation 20, the actual integrand I_A is approximated by a three-piece seventh-order Taylor series. The integrand of the left-hand side of Equation 20 can be rewritten as

$$I_T = \begin{cases} \sum_{k=0}^{7} \frac{z^k}{k!} I_A^{(k)}(0) & \text{for } 0 \leqslant z < \frac{L_s'}{4} \\ \sum_{k=0}^{7} \frac{[z - (L_s'/2)]^k}{k!} I_A^{(k)}\left(\frac{L_s'}{2}\right) & \text{for } \frac{L_s'}{4} \leqslant z < \frac{3L_s'}{4} \\ \sum_{k=0}^{7} \frac{(z - L_s')^k}{k!} I_A^{(k)}(L_s') & \text{for } \frac{3L_s'}{4} \leqslant z < L_s' \end{cases} \tag{23}$$

With the actual integrand I_A being substituted with the Taylor integrand I_T in Equation 20, the 'approximate' analytical form of the left-hand side of Equation 20 is achieved via integrating every Taylor polynomial term of I_T within the respective domain. The unknown L_s' can be solved by means of numerical approaches, and the axial deformation of the CFST column specimens can also be calculated. Due to bending of the specimen, its axial deformation differs when the LVDT (linear variable differential transformer) measurement position is changed and, for axial deformation along the loading axis, is given as

$$d_e = L_s - L_s' - (L - L_s)\cos\theta + \frac{L - L_s}{\cos\theta} \tag{24}$$

$$\cos\theta = \frac{1}{[1 + (u_{s,m}\pi/L_s')^2]^{1/2}} \tag{25}$$

The computation procedure in Matlab for the proposed non-linear analysis method is as follows.

(*a*) Read specimen data from Excel table.
(*b*) Calculate all the relevant coefficients for the material models.
(*c*) Input the value of $u_{s,m}$ and calculate the curvature ϕ_m at the mid-span of the specimen (initial value of L_s' is equal to L_s).
(*d*) Discretise the section into a finite number of fibre elements.
(*e*) Assume an initial neutral axis depth (e.g. $d_n = D/2$).
(*f*) Calculate the resultant section force P and internal moment M via Equations 11 and 12.
(*g*) Check whether Equation 19 is fulfilled.
(*h*) If not, the value of d_n should be renewed by numerical approximation techniques, and steps (f)–(g) are reiterated until the value of d_n fulfils Equation 19.
(*i*) Find the new value of L_s' via Equations 20–23.
(*j*) Calculate the new curvature ϕ_m' corresponding to the new L_s'.
(*k*) If $|\phi_m' - \phi_m| > 0{\cdot}001$ (in 10^{-3}/m), steps (*e*)–(*j*) are reiterated with the values of L_s' and $\phi_m$renewed by the most updated values of L_s' and ϕ_m' respectively, and the new L_s' and ϕ_m' are calculated in the next cycle.
(*l*) Increase the value of $u_{s,m}$ by $\Delta u_{s,m}$, and repeat steps (*c*)–(*l*) until failure deflection u_f is reached.
(*m*) Obtain the results of P, M, d_e, u_m and ϕ_m for each increment $\Delta u_{s,m}$.

The secant method (Liang, 2011) was applied as the numerical approximation technique mentioned in step (*h*), which will not be discussed in detail in this paper.

Determination of parameters a_1, a_2 and b_1

Parameters a_1, a_2 and b_1 in Equations 4 and 6 were determined by data fitting on existing experimental results from 87 specimens reported in previous research (Kilpatrick and Rangan, 1999; Lee *et al.*, 2011; Muciaccia *et al.*, 2011; Neogi *et al.*, 1969; O'Shea and Bridge, 2000; Portoles *et al.*, 2011, 2013; Xue *et al.*, 2012). As shown in Table 1, the ranges for the test parameters of the database are: effective column length L from 660 to 4670 mm; specimen length L_s from 578·5 to 4400 mm; outer tube diameter D from 76 to 600 mm; tube thickness t from 1·52 to 6 mm; yield strength of steel f_y from 256·4 to 517 MPa; cylinder concrete strength f_c from 26·4 to 112·7 MPa; eccentricity e from 9·4 to 300 mm.

Parameters a_1, a_2 and b_2 are adjusted to fulfil the following two criteria.

- The mean value of P_{model}/P_e of the 87 specimens should be as close to one as possible.
- The standard deviation should be the smallest.

Therefore, it was finally calculated that when $a_1 = 0{\cdot}0075$, $a_2 = 200$ and $b_1 = 15$, the mean value is equal to 1·00 and the standard deviation is 0·69 (see Table 1). The fitting results for P_{model}/P_e are shown in Figure 4, and Equations 4 and 6 can be rewritten as

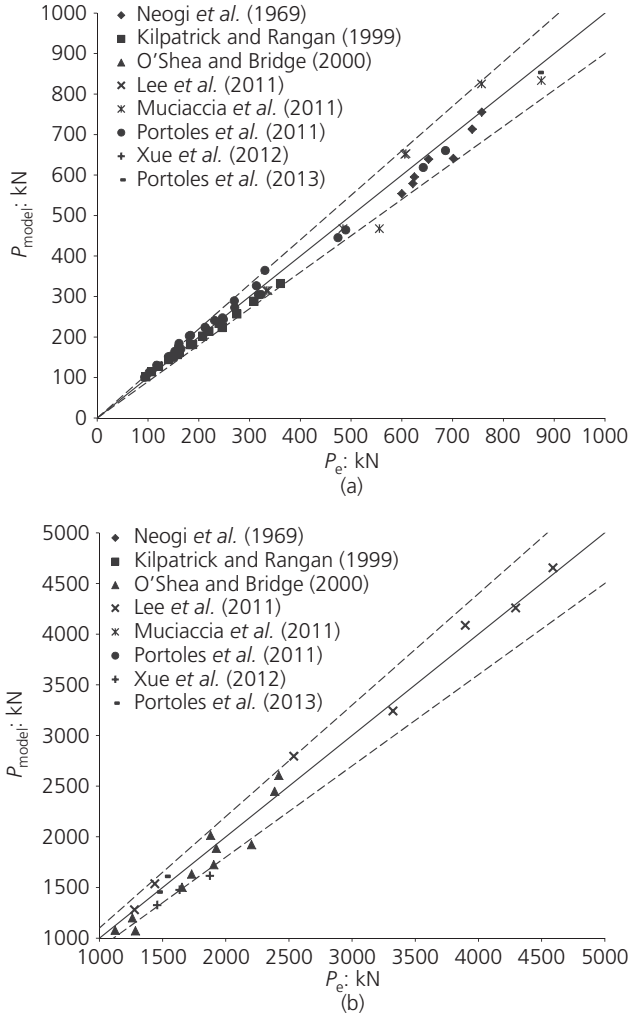

Figure 4. Predictions of maximum load by the proposed model

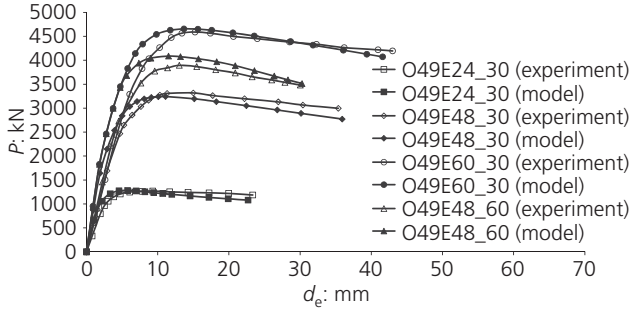

Figure 5. Eccentric load plotted against axial displacement at loading axis

$$26.\quad f_{r,avg} = 0{\cdot}0075\ln(200\rho + 1)f_y \leqslant \frac{2tf_y}{D-2t}$$

$$27.\quad \Phi = \exp(-15\phi)$$

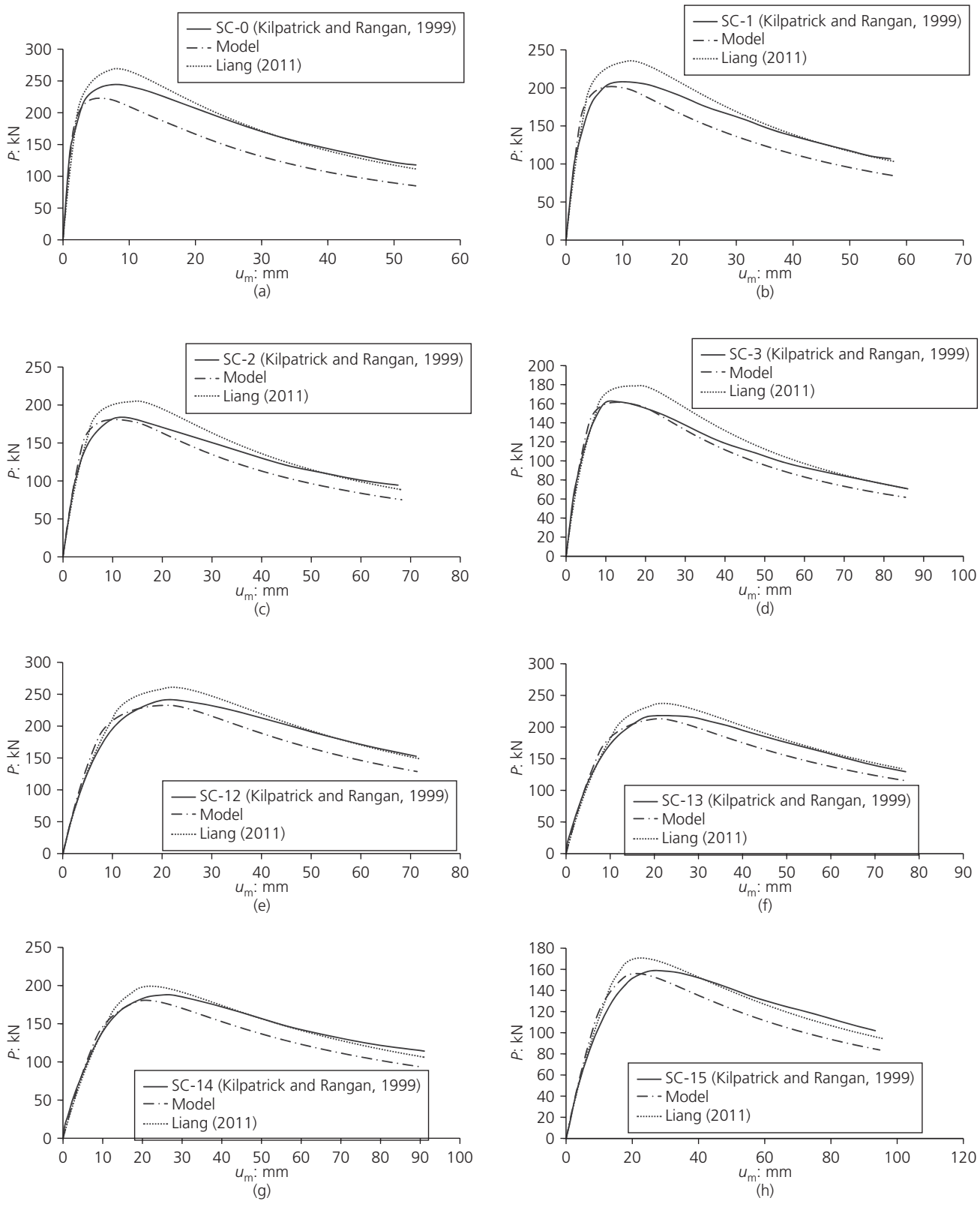

Figure 6. Eccentric load plotted against mid-span deflection

Behaviour of eccentrically loaded CFST columns

Eccentric load (P) against axial displacement at loading axis (d_e)

In the analysis method of Liang (2011) it was assumed that the effective (pin-to-pin) column length was unchanged during the loading process. Therefore, Liang's method cannot be used to predict the axial shortening of CFST under eccentric compression or the behaviour of eccentric load P against axial displacement at loading axis d_e.

The proposed non-linear analysis method in this paper provides dedicated steps to calculate axial shortening of the CFST columns, so that the P–d_e relation can be predicted. Among all the reviewed references, only Lee *et al.* (2011) managed to record the axial displacement at the eccentric loading axis of the CFST column tests through indirect measurement of two oppositely positioned LVDTs. For each load increment, the readings of the two LVDTs were logged and converted into a d_e value via the similar triangle relation, given that their horizontal distances to the loading axis were already known (Lee *et al.*, 2011).

Only four experimental P–d_e curves in the research of Lee *et al.* (2011) were presented without premature failure (O49E24_30, O49E48_30, O49E60_30 and O49E48_60) and these can be used to examine the proposed analysis method, as shown in Figure 5. In general, the predicted curves agree quite well with the experimental curves. The maximum predicted loads are basically very close to the experimental results (see Table 1). However, the predicted results are on the overestimation side in the ascending stage of all four specimens, which indicates that the axial displacement is underestimated. This could be due to the assumption of the half-sine wave deflection shape being conservative in terms of axial displacement prediction compared with the real shape.

Eccentric load (P) against mid-span deflection (u_m)

The experimental results of eight specimens reported by Kilpatrick and Rangan (1999) (SC-0 to SC-3 and SC-12 to SC-15) were used to examine the performance of the proposed analysis method in predicting the P–u_m relation of the eccentrically loaded circular CFST columns. As shown in Figure 6, the results from the proposed method agree very well with the experimental results in the ascending portion, but underestimation becomes quite obvious in the post-peak portion. On the other hand, Liang's model (Liang, 2011) gives significantly overestimated results in all specimens, which means its prediction is not on the safe side of the experimental curves.

There are several reasons why the proposed method underestimated the P–u_m relation in the post-peak portion. First of all, since Attard and Setunge's constitutive model for concrete (Attard and Setunge, 1996) is adopted in the proposed method, the reduction of concrete stress is more significant after the peak. As shown in Figure 7, despite that fact that the peak strength from

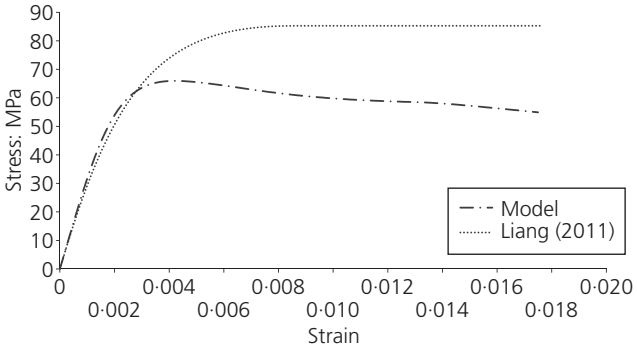

Figure 7. Comparison of different stress–strain relations for concrete in SC-1

Liang's curve is much larger than that of the adopted model, the reduction in concrete stress is zero after the peak for Liang's curve, while a drop in stress can be easily observed in the model adopted in this paper (Liang, 2011).

Mid-span internal moment (M) against mid-span curvature (ϕ_m)

The M–ϕ_m analysis is another important aspect of the proposed non-linear analysis method. However, due to the nature of the eccentrically loaded circular CFST columns, the most critical curvature normally takes place at the mid-span of the specimen, and it is impossible to apply direct measurements using tools such as inclinometers at that location to figure out the real-time curvature during experimental testing. Indirect measurement through several strain gauges at different depths of the mid-span section is an applicable approach, as used by Lee *et al.* (2011) in their experimental study. On the other hand, the moment can also be obtained by indirect measurement since secondary moments due to the P–Δ effect have to be considered. Normally the value of Δ is the mid-span deflection u_m, and it can be easily obtained by the LVDT placed at that location. Nonetheless, when the slenderness ratio of the specimen is small, u_m will develop slowly and will become susceptible to local buckling at that location. Access to experimental results for the M–ϕ_m relation is very limited, and the report of Lee *et al.* (2011) is one of the few that have presented experimental data. Unfortunately, the columns studied by Lee *et al.* (2011) had small slenderness ratios and some of them were reported to have local buckling issues near the mid-span.

Seven experimental tests conducted by Lee *et al.* (2011) were utilised to examine the performance of the proposed analysis method in predicting the M–ϕ_m relations of the eccentrically loaded circular CFST columns. Figure 8 shows that the M–ϕ_m relations of specimens O49E24_30, O49E48_30, O49E60_30 and O49E48_60 are predicted by the proposed concrete model with acceptable agreement, while the other specimens are significantly overestimated. O49E36_30, O49E48_30, O49E36_60 and O49E48_60 were noted to have local buckling issues at the mid-section part of the steel tube, which will increase the readings of

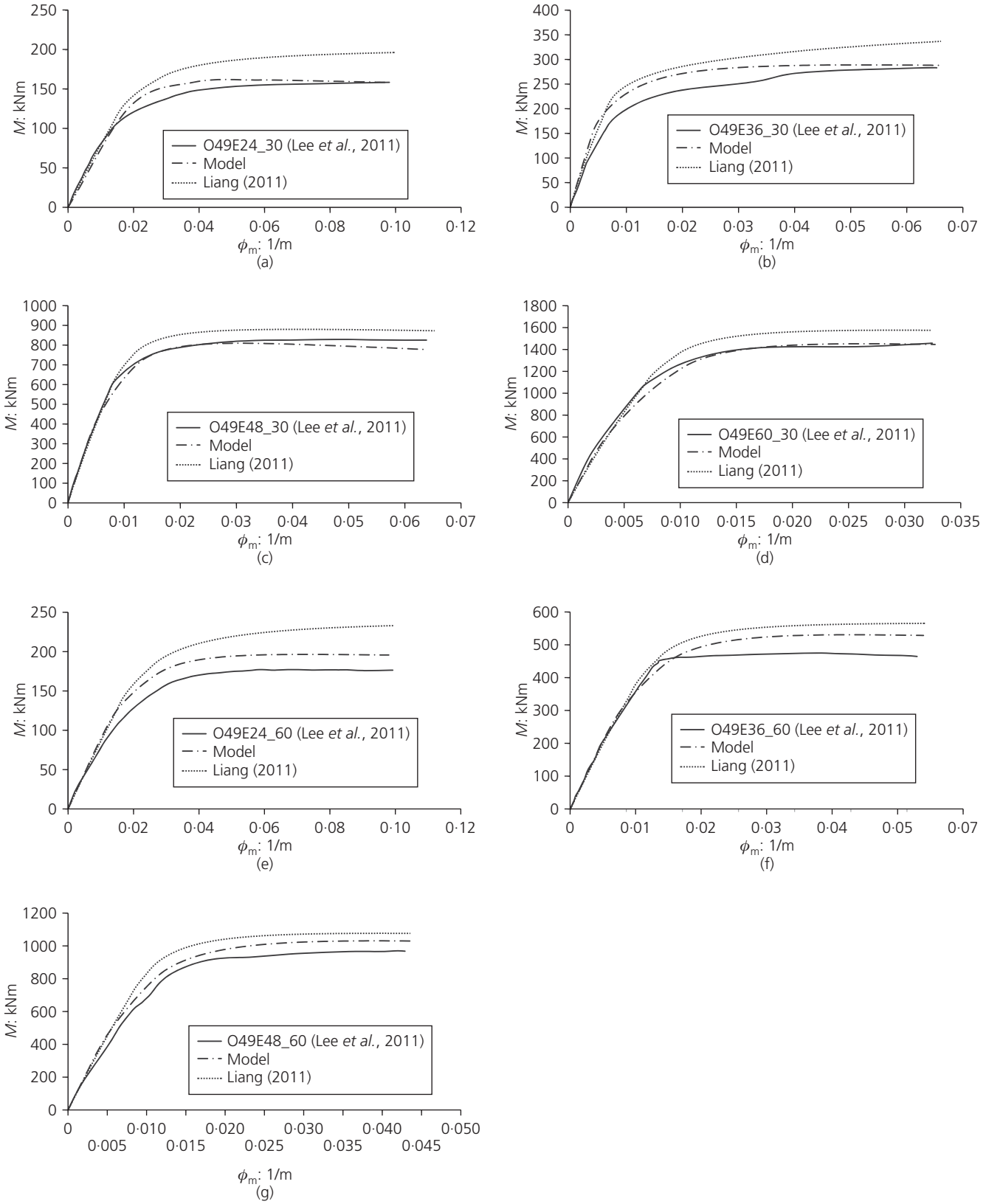

Figure 8. Moment plotted against mid-span curvature

the strain gauges and lower those of the LVDTs. As a result, the measured curvature is overstated (data point moves to the right) and the moment understated (data point moves downwards). In Figure 8, it is obvious that the experimental curves for the specimens with local bucking issues are not so smooth.

When compared with the curves obtained by the Liang (2011) model, the proposed analysis method gives results closer to the experimental data, with Liang's model overestimating the moment by a significant amount in all specimens.

Conclusions

Although there are several existing constitutive models for CFST concrete under axial load (Hatzigeorgiou, 2008; Hu *et al.*, 2003; Liang and Fragomeni, 2009), they may not predict the capacity of CFSTs under eccentric load accurately. Investigation of the analysis method for eccentrically loaded CFST columns proposed by Liang (2011), which incorporates the identical concrete model for the axial loading case from Liang and Fragomeni (2009), revealed that the method overestimates the capacity of eccentric loading on 87 specimens by 6% on average. Therefore, the concrete model for axial loading should not be used directly in the eccentric loading case, since the existence of curvature will reduce the effective confinement of the concrete.

This paper proposed a curvature-relevant model for CFST concrete in which $f_{r,avg}$ and $f_{r,eff}$ have two different concepts and can be calculated by Equations 26 and 27. The parameters a_1, a_2 and b_1 in Equations 26 and 27 were determined by data fitting on 87 CFST columns from various sources to be $a_1 = 0{\cdot}0075$, $a_2 = 200$ and $b_1 = 15$. The proposed method predicted the eccentric loading capacity of CFST columns with higher accuracy and precision.

An extra consideration in the proposed method is the capability of calculating the axial displacement of a CFST column during the loading process. In previous analysis methods (Liang, 2011; Neogi *et al.*, 1969), this variable has been neglected, so that it is impossible to estimate the P–d_e relation. The significance of carrying out this analysis is obvious, for example by helping an engineer estimate whether the axial displacement is excessive or not under certain coupled axial load and bending moment. Furthermore, the predicted results for the P–u_m relation were also presented. While the method of Liang (2011) shows distinct overestimation, the results obtained from the proposed analysis method illustrate satisfactory agreement with the experimental curves. On the other hand, the predicted results for the M–ϕ_m relation indicate that the proposed analysis method has a limitation of not being able to include local buckling effects. The proposed analysis method can therefore only be applied to compact CFST columns.

REFERENCES

Attard MM and Setunge S (1996) Stress–strain relationship of confined and unconfined concrete. *ACI Materials Journal* **93(5)**: 432–441.

Bridge RQ and O'Shea MD (1998) Behaviour of thin-walled steel box sections with or without internal restraint. *Journal of Constructional Steel Research* **47(1–2)**: 73–91.

Fujimoto T, Mukai A, Nishiyama I and Sakino K (2004) Behavior of eccentrically loaded concrete-filled steel tubular columns. *Journal of Structural Engineering* **130(2)**: 203–212.

Hajjar JF, Molodan A and Schiller PH (1998) A distributed plasticity model for cyclic analysis of concrete-filled steel tube beam–columns and composite frames. *Engineering Structures* **20(4–6)**: 398–412.

Hatzigeorgiou GD (2008) Numerical model for the behavior and capacity of circular CFT columns. Part I: Theory. *Engineering Structures* **30(6)**: 1573–1578.

Ho JCM and Pam HJ (2003) Inelastic design of low-axially loaded high-strength reinforced concrete columns. *Engineering Structures* **25(8)**: 1083–1096.

Ho JCM, Lam JYK and Kwan AKH (2010) Effectiveness of adding confinement for ductility improvement of high-strength concrete columns. *Engineering Structures* **32(3)**: 714–725.

Hu HT, Huang CS, Wu MH and Wu WM (2003) Nonlinear analysis of axially loaded concrete-filled tube columns with confinement effect. *Journal of Structural Engineering, ASCE* **129(10)**: 1322–1329.

Inai E, Mukai A, Kai M *et al.* (2004) Behavior of concrete-filled steel tube beam columns. *Journal of Structural Engineering* **130(2)**: 180–202.

Iveson SM, Litster JD, Hapgood K and Ennis BJ (2001) Nucleation, growth and breakage phenomena in agitated wet granulation process: a review. *Powder Technology* **117(1–2)**: 3–39.

Johansson M (2002) The efficiency of passive confinement in CFT columns. *Steel and Composite Structures* **2(5)**: 379–396.

Johansson M and Gylltoft K (2001) Structural behavior of slender circular steel–concrete composite columns under various means of load application. *Steel and Composite Structures* **1(4)**: 393–410.

Kayali O (2008) Fly ash lightweight aggregates in high performance concrete. *Construction and Building Materials* **22(12)**: 2393–2399.

Kilpatrick AE and Rangan BV (1999) Tests on high-strength concrete-filled steel tubular columns. *ACI Structural Journal* **96(2)**: 268–274.

Kupfer H, Hilsdorf K and Rusch H (1969) Behavior of concrete under biaxial stresses. *ACI Journal* **66(8)**: 656–666.

Kwan AKH and Fung WWS (2009) Packing density measurement and modelling of fine aggregate and mortar. *Cement and Concrete Composites* **31(6)**: 345–357.

Kwan AKH and Ng IYT (2010) Improving performance and robustness of SCC by adding supplementary cementitious materials. *Construction and Building Materials* **24(11)**: 2260–2266.

Lee SH, Uy B, Kim SH, Choi YH and Choi SM (2011) Behavior of high-strength circular concrete-filled steel tubular (CFST) column under eccentric loading. *Journal of Constructional Steel Research* **67(1)**: 1–13.

Liang QQ (2011) High strength circular concrete-filled steel tubular slender beam–columns. Part I: Numerical analysis. *Journal of Constructional Steel Research* **67(2)**: 164–171.

Liang QQ and Fragomeni S (2009) Nonlinear analysis of circular concrete-filled steel tubular short columns under axial loading. *Journal of Constructional Steel Research* **65(12)**: 2186–2196.

Mander JB, Priestly JN and Park R (1988) Theoretical stress–strain model for confined concrete. *Journal of Structural Engineering, ASCE* **114(8)**: 1804–1826.

Menétrey P and Willam KJ (1995) Triaxial failure criterion for concrete and its generalization. *ACI Structural Journal* **92(3)**: 311–318.

Muciaccia G, Giussani F, Rosati G and Mola F (2011) Response of self-compacting concrete filled tubes under eccentric compression. *Journal of Constructional Steel Research* **67(5)**: 904–916.

Neogi PK, Sen HK and Chapman JC (1969) Concrete-filled tubular steel columns under eccentric loading. *The Structural Engineer* **47(5)**: 187–195.

Oliveira WL, Nardin SD, Cresce El Debs AL and El Debs MK (2010) Evaluation of passive confinement in CFT columns. *Journal of Constructional Steel Research* **4(66)**: 487–495.

O'Shea MD and Bridge RQ (2000) Design of circular thin-walled concrete-filled steel tubes. *Journal of Structural Engineering, ASCE* **126(11)**: 1295–1303.

Portoles JM, Romero ML, Bonet JL and Filippou FC (2011) Experimental study of high strength concrete-filled circular tubular columns under eccentric loading. *Journal of Constructional Steel Research* **67(4)**: 623–633.

Portoles JM, Serra E and Romero ML (2013) Influence of ultra-high strength infill in slender concrete-filled steel tubular columns. *Journal of Constructional Steel Research* **86**: 107–114.

Prion HG and Boehme J (1994) Beam–column behaviour of steel tubes filled with high strength concrete. *Canadian Journal of Civil Engineering* **21(2)**: 207–218.

Richart FE, Brandtzaeg A and Brown RL (1928) *A Study of the Failure of Concrete Under Combined Compressive Stresses*. Engineering Experimental Station, University of Illinois, Champaign, IL, USA, Bulletin 190.

Richart FE, Brandtzaeg A and Brown RL (1929) *Failure of Plain and Spirally Reinforced Concrete in Compression*. Engineering Experimental Station, University of Illinois, Champaign, IL, USA, Bulletin 185.

Suthansa K, Ge H and Usami T (2001) Uniaxial stress–strain relationship of concrete confined by various shaped steel tubes. *Engineering Structures* **23(10)**: 1331–1347.

Tang J, Hino S, Kuroda I and Ohta T (1996) Modeling of stress–strain relationships for steel and concrete in concrete filled circular steel tubular columns. *JSSC Journal of Construction Steel* **3(11)**: 35–46.

Tao Z, Han LH and Wang DY (2007) Experimental behaviour of concrete-filled stiffened thin-wall steel tubular columns. *Thin-Walled Structures* **45(5)**: 517–527.

Uy B (2000) Strength of concrete-filled steel box columns incorporating local buckling. *Journal of Structural Engineering, ASCE* **126(3)**: 341–352.

Wong HHC and Kwan AKH (2008a) Packing density of cementitious materials: Part 1 – measurement using a wet packing method. *Materials and Structures* **41(4)**: 689–701.

Wong HHC and Kwan AKH (2008b) Packing density of cementitious materials: measurement and modelling. *Magazine of Concrete Research* **60(3)**: 165–175.

Xue JQ, Briseghella B and Chen BC (2012) Effects of debonding on circular CFST stub columns. *Journal of Constructional Steel Research* **69(1)**: 107–114.

Yu T, Teng JG, Wong YL and Dong SL (2010) Finite element modeling of confined concrete – I: Drucker–Prager type plasticity model. *Engineering Structures* **32(3)**: 665–679.